The sintering and mechanical behavior of hydroxyapatite with bioglass additions

D. C. TANCRED, A. J. CARR*
Bioengineering Research Center, Department of Mechanical Engineering, University College Dublin, Belfield, Dublin 4, Ireland
E-mail: alun.j.carr@ucd.ie

B. A. O. MCCORMACK
Department of Mechanical and Electronic Engineering, Institute of Technology Sligo, Ballinode, Co. Sligo, Ireland

There is increasing interest in the potential of composites of hydroxyapatite with phosphate- or silicate-based bioactive glasses, and certain of these glass additions have been found, in previous work, to aid densification and form a mechanically-reinforced, bioactive material; in particular, large improvements in flexural strength and fracture toughness were obtained through the addition of small amounts of phosphate glass. Less is known about the mechanical behavior of HA/bioglass composites, although *in vivo* studies by other workers have shown encouraging biological results. In this investigation, the sintering behavior, mechanical properties, and microstructure of composites of HA with up to 50 wt % glass, were analyzed. X-ray diffraction showed the phase composition of sintered composites with up to 5 wt % added bioglass to be non-stoichiometric HA with α-TCP or β-TCP. Phase analysis of composites containing higher glass additions was impracticable due to peak broadening and overlap, although reaction products, at the highest glass additions and sintering temperatures, may include wollastonite-2M and β-$Na_2Ca_4(PO_4)_2SiO_4$. Sintered density, and mechanical properties other than fracture toughness, showed no significant improvement over HA.

1. Introduction

There have been several attempts to combine hydroxyapatite (HA) with glasses of different composition, in order to produce composites with improved mechanical or bioactive properties. Composites formed by sintering of HA with small glass additions, may exhibit greatly improved mechanical properties, largely due to improved densification through the presence of a liquid phase during sintering [1]. Reaction between the HA and the glass may occur at sintering temperatures, and the final phase composition can be altered by varying the glass composition and the sintering temperature.

Two main glass types have previously been investigated as potential sintering aids for HA. Addition of some phosphate glasses ($CaO–P_2O_5$) can produce a significant improvement in mechanical properties [1–3]. Close chemical similarity to HA and tricalcium phosphate (TCP) ensures that such composites consist only of calcium phosphate phases; they are, consequently, likely to be biocompatible and possibly bioactive [4, 5]. Silicate-based glasses have also been used to form composites with HA, either as a sintered monolithic body, or as a plasma-sprayed coating [6, 7]. Composites containing large silicate glass contents may be composed of HA particles dispersed in either a bioinert glass [8, 9] or in a bioactive bioglass matrix [6, 10]. Alternatively, small additions (of up to 5 wt % glass) have been added to HA as a sintering aid, to improve densification, mechanical properties, and possibly bioactivity [11, 12].

The biological response to HA/bioglass composites is still unclear. *In vitro* studies of composites containing small amounts of bioglass showed that although the period immediately following immersion in simulated body fluid is characterized by significant surface dissolution, the composites may form an apatite surface layer [12, 13], a property usually considered indicative of a bioactive material. The time required for formation of an apatite layer was shorter than for sintered HA, indicating higher bioactivity [12].

In vitro studies have shown that composites with very high bioglass levels (70–90 wt %) are bioactive, and may bond to bone [14]. *In vivo* studies using a subchondral bone defect in a rabbit model for the same materials containing 70 wt % bioglass showed that bonding to bone occurred in as little as 6 weeks and that the material promoted chondrogenesis [15]; however, substantial degradation of the implant occurred over a 12 week

*Author to whom all correspondence should be addressed.

period. Granules of the same HA/bioglass composition implanted in metaphyseal cavities in rabbit models performed similarly to autograft over short time periods, with a better response over longer times [16].

In this work, HA composites containing 0–50 wt % bioglass additions, were investigated over a range of sintering temperatures (T_{sinter}), to allow determination of their phase composition, microstructure, and mechanical properties. This provides a quantitative assessment of the properties of such composites across a wide range of glass additions, allowing comparison with other HA/glass composite systems previously studied [1, 3, 11].

2. Materials and methods

2.1. Powder preparation

Synthetic hydroxyapatite was prepared by reaction of calcium hydroxide and orthophosphoric acid in aqueous solution [17], according to the equation:

$$6H_3PO_{4_{(aq.)}} + 10Ca(OH)_{2_{(aq.)}} = Ca_{10}(PO_4)_6(OH)_{2_{(s)}} + 18H_2O_{(l)} \quad (1)$$

Reagent grade $Ca(OH)_2$ (96% pure, Merck, Darmstadt, Germany), AnalaR grade H_3PO_4 (85%, BDH, Poole, UK), and deionized water, were used. The reaction was carried out at 85 °C, with the pH maintained above 9.5 by the addition of ammonia solution (GPR grade, BDH). X-ray diffractometry (XRD) of powders, calcined in air at temperatures between 900 °C and 1350 °C, showed that the synthesized HA contained no secondary phase and was stable up to at least 1350 °C.

A bioglass previously used by Kangasniemi *et al*. [18], of composition (in mol %) 52.6 SiO_2, 25.8 Na_2O, 13.1 CaO, 4.7 P_2O_5, 0.5 Al_2O_3, 3.3 B_2O_3, was prepared. Reagent grade powders of silica (99.9% pure, Tilcon Industrial Materials, Stoke-on-Trent, UK), sodium carbonate (99.5%, BDH), calcium carbonate (98%, Aldrich, Gillingham, UK), phosphorous pentoxide (97%, Merck), boric acid (99.8%, Merck), and alumina (99.5%, British Alcan Chemicals, Burntisland, UK), were dry-mixed by tumbling in a 1 l polypropylene Nalgene pot (Nalge Nunc International, Rochester, NY, USA) on ball mill rollers, and melted at 1370 °C for 2 h in a sintered mullite crucible (Zedmark Refractories, Dewsbury, UK). The resulting melt was quenched in water, collected, and dried.

HA and bioglass were separately dry ball-milled for 1 h in a 5 l alumina milling pot (Lodge Ceramics, Rugby, UK) using 12.5 mm diameter Mg-partially-stabilized-zirconia (Mg-PSZ) cylpeb media (Mandoval, Lightwater, UK) and screened to -45 μm using brass BS410:1986 test sieves (Endecotts, London, UK), giving stock powders.

HA, and HA/bioglass composite powders containing 2.5, 5, 10, 25, and 50 wt % glass, were prepared by wet ball-milling 60 g batches in 180 ml isopropyl alcohol (general use grade, 99.5% pure, Romil, Loughborough, UK) for 24 h, using 500 ml polypropylene Nalgene pots containing approximately 650 g of 7 mm Mg-PSZ cylpeb media. Slips were recovered and passed through a 38 μm test sieve, dried at 70 °C, and then passed through a 106 μm test sieve to break up agglomerates formed on drying.

2.2. Sample preparation

Powders were mixed with 4 wt % of an organic binder based on polyvinyl acetate and polyethylene glycol (Bindemittel B11/V, Mahler Dienstleistungs, Esslingen, Germany), to provide lubrication during pressing and to improve the green strength. Disc samples were uniaxially cold-pressed in a 25 mm diameter tool steel die at 120 MPa, using 2 g of powder per sample. The binder was allowed to cure, and was subsequently removed by heating at 2 °C min^{-1} to 350 °C. Sintering was carried out in a muffle furnace, using a heating rate of 4 °C min^{-1} up to sintering temperature, which was held for 3 h, followed by cooling at 4 °C min^{-1} down to room temperature.

2.3. Density measurement

Specimen bulk density (ρ_{bulk}) was measured by application of Archimedes' principle. A mercury balance method was used, in which the upthrust from immersing the specimen in a mercury bath was measured using a top-pan balance (model GT4800, Ohaus, Florham Pk, NJ, USA), allowing densities to be determined to better than ± 0.02 g cm^{-3}. Ninety-five per cent confidence limits were calculated for each mean density [19].

2.4. XRD analysis

X-ray diffraction studies were carried out using a System 642 Guinier diffractometer (Huber Diffraktionstechnik, Rimsting, Germany), operating in subtractive transmission mode; Huber G600 software was used for control and data acquisition. Radiation was pure monochromatic $CuK\alpha_1$ ($\lambda = 1.54056$ Å), focused using a quartz Guinier–Johansson monochromator. Data were recorded over the range $\theta = 0$–$50°$ with a 0.02° step size, a count time of 5 s, and a counter slit width of 0.2 mm. Si powder (pure element grade, 99.5% pure, Johnson Matthey Alfa Products, Karlsruhe, Germany) was added to all samples as an internal standard (at a constant level of 10 wt %), to allow correction of the peak positions [20]. The internal standard was also used to compensate for the variable X-ray absorption coefficient of the multi-phase mixtures, during quantitative phase determination [21–23]. Lattice parameters were calculated using Cohen's method [24], and are quoted with 95% confidence limits.

In order to allow quantitative analysis of the HA and β-TCP contents, calibration constants were determined. HA powder was synthesized as described in Section 2.1 (above) and calcined in air at 900 °C; β-TCP powder had a purity greater than 98% (purum p.a. grade, Fluka Chemie, Buchs, Switzerland) and was also calcined at 900 °C. Calibration samples were prepared by mixing these two powders in various proportions between 0 and 100% β-TCP, together with 10 wt % of Si internal standard, using an agate mortar and pestle. Diffraction traces over the range $\theta = 10$–$20°$ were produced using the conditions specified above, and the integrated intensities determined for the Si 111 (I_{Si}), HA 211 (I_{HA}), and β-TCP 02 · 10 ($I_{\beta\text{-TCP}}$) reflexions. Regression models were established from the following relationships:

$$\frac{x'_A}{x_{Si}} = k_A \cdot \frac{I_A}{I_{Si}} \quad (2)$$

and

$$x_A = \frac{x'_A}{(1 - x_{Si})} \quad (3)$$

where k_A is the calibration constant for phase A, x_A is the mass fraction of A in the powder mixture to be analyzed, x'_A is the mass fraction of A in the mixture after x_{Si} internal standard has been added, and I_A is the integrated intensity of the selected reflexion for A (for more details see, e.g. Klug and Alexander [21]). From this, it can be seen that

$$w_A = k'_A \cdot \frac{I_A}{I_{Si}} \quad (4)$$

where w_A is the weight percentage of phase A in the mixture without internal standard additions and (for a constant level of internal standard addition; e.g. 10 wt % Si in the present case) $k'_A = 100 k_A x_{Si}/(1 - x_{Si})$.

Minitab statistical analysis software (version 8.1; Minitab, State College, PA, USA) was used to fit the regression models (w_{HA} vs I_{HA}/I_{Si}, $w_{\beta\text{-TCP}}$ vs $I_{\beta\text{-TCP}}/I_{Si}$) to the data. The models were calculated to be:

$$w_{HA} = 32.86(0.37) \times \frac{I_{HA}}{I_{Si}}, \qquad r^2 = 0.999 \quad (5)$$

$$w_{\beta\text{-TCP}} = 40.52(0.44) \times \frac{I_{\beta\text{-TCP}}}{I_{Si}}, \qquad r^2 = 0.999 \quad (6)$$

where the standard deviations of the slopes of the regression lines are in parentheses, and r^2 is the coefficient of determination. Minitab also calculated 95% prediction intervals [19] for the HA and β-TCP contents which were derived from the regression models.

The validity of the internal standard method for quantitative phase analysis depends on the absence of amorphous material in the powders used to produce the calibration constants; this was assumed to be the case for the calcined powders used in the present work.

Estimation of α-TCP content was attempted using the I/I_{cor} ratios from the JCPDS Powder Diffraction File (PDF; JCPDS–ICDD, Swarthmore, PA, USA) for α-TCP and Si, applying the relationship given by Monaco [22]:

$$x'_{\alpha\text{-TCP}} = x_{Si} \cdot \frac{k_{Si}}{k_{\alpha\text{-TCP}}} \cdot \frac{I_{\alpha\text{-TCP}}}{I_{Si}} \quad (7)$$

where $k_{\alpha\text{-TCP}}$ is $I/I_{cor} = 0.44$ for the α-TCP 034 reflexion (PDF card No. 29-359) and k_{Si} is $I/I_{cor} = 4.70$ for the Si/111 reflexion (card No. 27-1402). This procedure was found to be unsatisfactory, producing substantial overestimates of the mass fraction of α-TCP (giving a total crystalline material content substantially exceeding 100 wt % in some cases). This could be due to the α-TCP material in the PDF having a low crystallinity. Accordingly, $I_{\alpha\text{-TCP}}/I_{Si}$ values (based on integrated intensities) are reported, to permit calculation of the mass fraction of α-TCP when a more accurate I/I_{cor} becomes available.

2.5. Microscopy

All samples for microstructural analysis were surface ground using silicon carbide grinding paper, finishing with grade 4000. Samples were then polished for 5 min, using an OP-NAP cloth (Struers, Copenhagen, Denmark), Metadi 3 μm aerosol diamond compound (Buehler, Lake Bluff, IL, USA), and deionized water as a lubricant.

Composites containing 2.5 and 5 wt % glass additions were etched for 10 s using 0.1 M lactic acid (extra pure grade, Merck). For composites based on higher bioglass additions, attempts to reveal a microstructure (using lactic acid, HCl (GPR grade, BDH), and thermal etching) were unsuccessful. Fracture surfaces for these higher-glass composites were examined, to investigate the development of microstructure during sintering. Micro structures and fracture surfaces were studied using a JSM-35C (JEOL, Tokyo, Japan) scanning electron microscope (SEM) operating at 25 kV.

2.6. Mechanical testing

Biaxial flexural strength (σ_F) was measured using a disc bend test method [25]. The samples were ground on the tensile face using a surface grinding machine with a resin-bonded diamond wheel; R_a was measured using a Surtronic 3P Tallysurf (Taylor-Hobson, Leicester, UK), and in all cases lay in the range 1–1.5 μm. The load at failure was measured using a model 6000S mechanical testing machine (Lloyd Instruments, Fareham, UK), fitted with a 500 N load cell, and a cross-head speed of 0.5 mm min^{-1}.

Hardness (H_V) was measured by Vickers indentation, using an AVK-C2 hardness tester (Akashi division of Mitutoyo, Kanagawa, Japan), a 2 kgf load, and a 15 s dwell time.

Fracture toughness (K_{Ic}) was determined by measurement of the radial crack lengths (half the crack-tip to crack-tip distance) propagating from the Vickers indentation [26]; if a load of 2 kgf was found to be insufficient to develop a well-defined radial crack system, fresh indentations at successively higher loads were carried out until adequate cracks were formed.

Where possible, a sample size of at least 6 was used for each mechanical test. Ninety-five per cent confidence intervals were calculated for each set of measurements [19].

3. Results

3.1. XRD analysis

In all cases, reaction occurred between the HA and the bioglass addition, resulting in a reduction of HA content, and the formation of additional phases such as α- and β-TCP. The XRD results are summarized in Table I, and in Figs 1 and 2. Lattice parameters of HA showed appreciable deviations from those of stoichiometric HA, at all levels of glass addition.

The data presented in Fig. 1(b) represent the crystalline phase content, corrected for the initial glass addition: the weight percentage of each phase (from Fig. 1(a)) has been divided by $1 - x_{glass}$ (where x_{glass} is the mass fraction of glass added to the HA); i.e., the corrected HA content, where no reaction had occurred with the glass,

TABLE I XRD phase analysis data for composites of HA with the addition of 2.5, 5, 10, 25, and 50 wt % bioglass (with 95% prediction limits)

Bioglass (wt %)	T_{sinter} (°C)	HA (wt %)	β-TCP (wt %)	HA corr.[a] (wt %)	β-TCP corr.[a] (wt %)	$x_{HA}/x_{\beta\text{-TCP}}$	$I_{\alpha\text{-TCP}}/I_{Si}$[b]
2.5	1200	68.5 ± 5.7	10.6 ± 3.2	70.2 ± 5.8	10.9 ± 3.3	6.0 ± 1.1	n.p.[c]
	1250	65.2 ± 5.6	6.7 ± 3.2	66.8 ± 5.8	6.8 ± 3.3	9.1 ± 1.1	n.p.
	1300	73.1 ± 5.7	n.p.	75.0 ± 5.8	n.p.	—	0.158
	1350	55.3 ± 5.6	n.p.	56.8 ± 5.7	n.p.	—	0.357
5	1200	63.2 ± 5.6	20.3 ± 3.2	66.5 ± 5.9	20.8 ± 3.3	2.9 ± 1.1	n.p.
	1250	50.2 ± 5.5	16.3 ± 3.2	52.8 ± 5.8	16.8 ± 3.3	2.9 ± 1.1	n.p.
	1300	47.0 ± 5.5	n.p.	49.4 ± 5.8	n.p.	—	0.624
	1350	36.6 ± 5.5	n.p.	38.6 ± 5.7	n.p.	—	0.785
10	1100	4.2 ± 5.4	57.4 ± 3.5	4.6 ± 6.0	58.9 ± 3.6	0.1 ± 1.1	n.p.
	1150	39.6 ± 5.5	37.2 ± 3.3	44.0 ± 6.1	38.2 ± 3.4	1.0 ± 1.1	n.p.
	1200	53.3 ± 5.5	19.1 ± 3.2	59.2 ± 6.2	19.6 ± 3.3	2.6 ± 1.1	n.p.
	1250	40.4 ± 5.5	14.3 ± 3.2	44.9 ± 6.1	14.7 ± 3.3	2.6 ± 1.1	n.p.
25	1050	25.1 ± 5.4	n.p.	33.4 ± 7.2	n.p.	—	n.p.
	1100	19.0 ± 5.4	1.5 ± 3.2	25.3 ± 7.2	1.5 ± 3.3	11.8 ± 1.1	n.p.
	1150	30.6 ± 5.4	15.9 ± 3.2	40.8 ± 7.2	16.3 ± 3.3	1.8 ± 1.1	n.p.
	1200	30.0 ± 5.4	12.6 ± 3.2	40.1 ± 7.2	12.9 ± 3.3	2.2 ± 1.1	n.p.
50	600	20.8 ± 5.4	n.p.	41.6 ± 10.8	n.p.	—	n.p.
	700	24.8 ± 5.4	1.5 ± 3.2	49.7 ± 10.8	1.5 ± 3.3	15.8 ± 1.1	n.p.
	800	31.4 ± 5.4	15.3 ± 3.2	62.7 ± 10.9	15.7 ± 3.3	1.9 ± 1.1	n.p.
	900	n.p.	1.1 ± 3.2	n.p.	1.1 ± 3.3	0.0 ± 1.1	n.p.

[a]Weight per cent of phase corrected for glass addition by dividing by $1 - x_{glass}$.
[b]Ratio of integrated intensities of α-TCP 034 and Si 111 reflexions.
[c]Phase not present.

would be 100% by weight of the total crystalline material.

3.1.1. 2.5 and 5 wt % glass additions

The only crystalline phases evident in the materials with 2.5 and 5 wt % bioglass added, were HA, α-TCP, and β-TCP. Samples sintered at 1200 °C and 1250 °C both formed β-TCP as the sole crystalline reaction product, with about twice the quantity of β-TCP being formed in the material containing a 5 wt % glass addition, resulting in a lower HA:β-TCP ratio (Table I, and Figs 1 and 2). Less β-TCP was formed at the higher temperature, for both glass contents: a decrease of 38% for the 2.5 wt % material, and a decrease of 19% for the 5 wt % material.

On raising the sintering temperature to 1300 °C, the β-TCP was replaced by α-TCP in both materials. For the 2.5 wt % glass composites, the quantity of α-TCP more than doubled when the sintering temperature was increased to 1350 °C; for the 5 wt % glass material, a smaller rise of about 25% was observed.

With both 2.5 and 5 wt % bioglass additions, the trend was for both the HA content, and also the total HA + β-TCP content, to decrease with increasing temperature (Fig. 1), through increased reaction with,

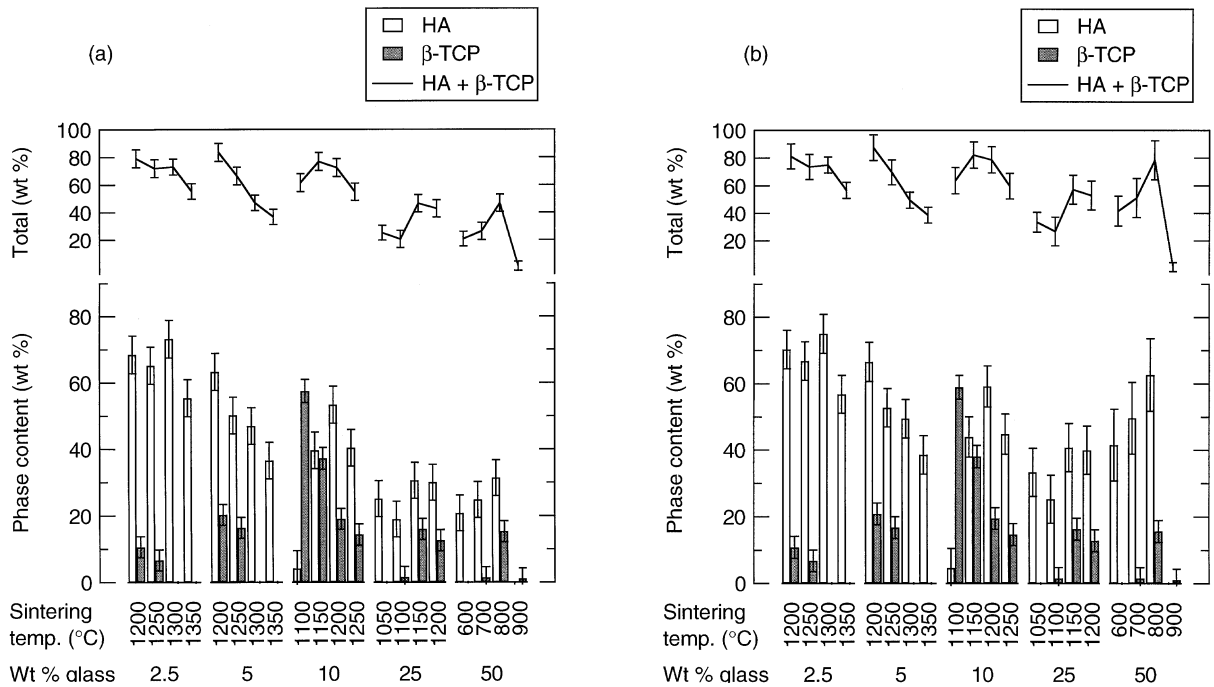

Figure 1 Variation, with sintering temperature, of weight percentages of crystalline HA and β-TCP, in composites containing additions of 2.5, 5, 10, 25, and 50 wt % of bioglass: (a) absolute values, (b) corrected for glass addition (with 95% prediction intervals).

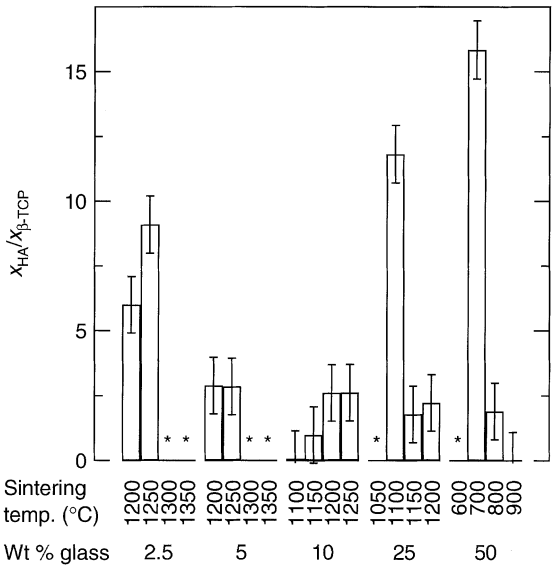

Figure 2 Ratio of HA to β-TCP in composites containing additions of 2.5, 5, 10, 25, and 50 wt % of bioglass (with 95% prediction intervals); * indicates that no β-TCP was present.

and dissolution in, the bioglass. The exception to this was the material containing 2.5 wt % bioglass, sintered at 1300 °C, which had an unexpectedly high HA content; the HA also had a slightly low *a*-dimension (Fig. 3), significantly smaller than that of the HA in material sintered at 1350 °C ($p < 0.0001$). However, the HA *c*/*a*-ratio for the 2.5 wt % bioglass material, sintered at 1300 °C, was not significantly different from that sintered at 1350 °C ($p > 0.05$). It should be noted from Fig. 3 that the *c*-dimension of the pure HA remains almost constant with sintering temperature, changes in *c*/*a* stemming almost entirely from the reduction in *a*; in the composite materials, there is a substantial increase in *c* alongside the reduction in *a*, as T_{sinter} increases.

The *c*/*a* ratio for HA (Fig. 4), in materials with both 2.5 and 5 wt % glass, was in all cases somewhat higher than for pure HA, and as for pure HA, the value of *c*/*a* rose with increasing sintering temperature, although at a higher rate.

3.1.2. 10 wt % glass addition

At the lowest sintering temperature (1100 °C), only a small quantity of HA was present, increasing by a factor of 10 at 1150 °C, rising about one-third further at 1200 °C, and finally falling by almost one-quarter at the highest sintering temperature of 1250 °C (Table I and Fig. 1). The sum of the HA and β-TCP contents followed a similar trend, reaching a maximum at 1150 °C rather than 1200 °C.

For these materials, the β-TCP content was found to decrease with increasing sintering temperature, the mass fraction of β-TCP at a temperature of 1100 °C being four times that of the same material sintered at 1250 °C. The HA:β-TCP ratio (Fig. 2) was found to rise with sintering temperature, leveling off at the two highest temperatures. At sintering temperatures of 1200 °C and 1250 °C, the quantities of HA and β-TCP formed (after adjustment for initial glass content) were similar to those in the 5 wt % glass material at the same temperatures, giving almost identical HA:β-TCP ratios (Fig. 2).

The change in phase composition may be seen in Fig. 5. No α-TCP was observed in these samples. It was not possible to identify other phases present, despite the high resolution of the Guinier diffractometer, due to peak broadening and overlap. These effects also made it impossible to determine the *a* and *c* values for HA with any degree of precision.

3.1.3. 25 and 50 wt % glass additions

Analysis of these samples was difficult due to the large amount of peak broadening, and also peak overlap with unidentified phases, in most cases.

For both materials, β-TCP did not form at the lowest

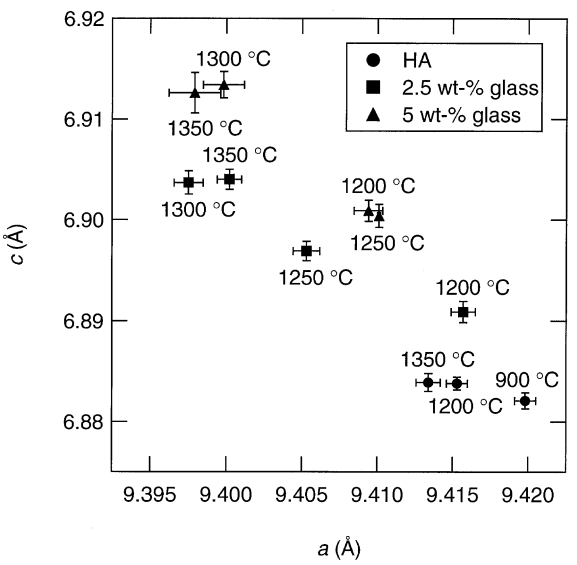

Figure 3 Variation in lattice parameters of HA, both for pure HA, and for HA/glass composites containing additions of 2.5 and 5 wt % of bioglass (with 95% confidence intervals).

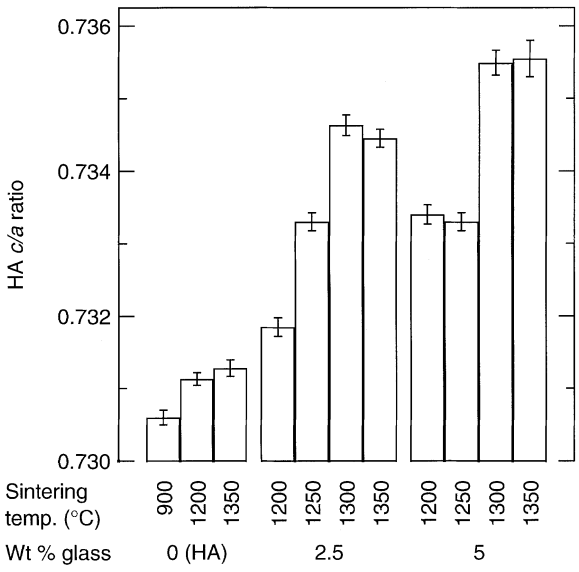

Figure 4 Variation in *c*/*a* ratio of HA, both for pure HA, and for HA/glass composites containing additions of 2.5 and 5 wt % of bioglass (with 95% confidence intervals).

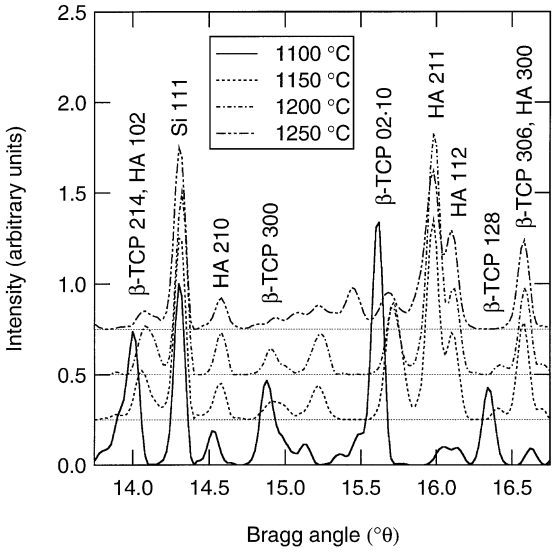

Figure 5 Overlay of the XRD traces for HA + 10 wt % bioglass material, showing phase variation with sintering temperature (intensities normalized with respect to the internal standard).

sintering temperature (1050 °C for 25 wt % glass, 600 °C for 50 wt %). β-TCP was strongly evident in the 25 wt % glass material sintered at the two highest temperatures (1150 °C and 1200 °C), but was only strongly present in the 50 wt % glass sample sintered at 800 °C; it existed only in trace quantities, or was completely absent, in other specimens. The HA:β-TCP ratio for the 25 wt %, 1200 °C sample, was similar to those for the 5 wt % and 10 wt %, 1200 °C materials (Fig. 2).

The general trend was for HA content to rise with increasing temperature, although the amount of HA in the 25 wt %, 1100 °C sample, was somewhat low. The composite containing 50 wt % bioglass, sintered at 900 °C, was the only sample, out of all the compositions prepared, which contained no HA after sintering, indicating complete reaction with the glass. It was not possible to identify any of the phases other than HA and β-TCP in the 25 wt % glass composites, or in the 50 wt %, 600 °C and 700 °C samples; there was possibly some β-$Na_2Ca_4(PO_4)_2SiO_4$ (PDF card No. 32-1053) formed as one of the additional phases in the 50 wt %, 800 °C specimen, and possibly both wollastonite-2M (card No. 27–88) and β-$Na_2Ca_4(PO_4)_2SiO_4$ in the 900 °C material.

3.2. Density

Bulk densities of all the sintered materials are given in Table II, and their variation with sintering temperature is shown in Fig. 6. Generally, density rose with increasing sintering temperature, although the density of the sample with 10 wt % bioglass, sintered at 1150 °C, was anomalously low. The 50 wt %, 900 °C composite, also had a low density; this may be associated with the complete reaction of HA with the bioglass.

Fig. 7 is a graph of the maximum bulk density (ρ_{max}) obtained in each series of materials; also shown on the graph is a line representing the rule-of-mixtures density (ρ_{theor}) for HA ($\rho_{HA} = 3.15\,g\,cm^{-3}$, from PDF card No. 9-432) and the bioglass ($\rho_{glass} = 2.60\,g\,cm^{-3}$, present work) mixtures.

If all of the materials (i) sinter to the same level of

TABLE II Bulk density and mechanical properties, for pure HA, and for composites of HA with the addition of 2.5, 5, 10, 25 and 50 wt % bioglass (with 95% confidence limits)

Bioglass (wt %)	T_{sinter} (°C)	ρ_{bulk} (g cm^{-3})	H_V (HV2)	K_{Ic} (MPa M$^{1/2}$)	σ_F (MPa)
0 (HA)	1150	3.04 ± 0.02	502.5 ± 11.0	0.67 ± 0.07	20.5 ± 4.4
	1200	3.05 ± 0.02	522.3 ± 25.1	0.56 ± 0.04	31.4 ± 4.4
	1250	3.08 ± 0.02	523.7 ± 19.4	0.67 ± 0.04	17.9 ± 2.5
	1300	3.08 ± 0.02	509.0 ± 11.5	0.74 ± 0.03	20.9 ± 2.7
2.5	1200	2.03 ± 0.02	217.5 ± 4.7	0.96 ± 0.06	20.0 ± [a]
	1250	2.46 ± 0.01	398.8 ± 12.0	0.96 ± 0.05	35.7 ± 6.4
	1300	2.87 ± 0.03	411.6 ± 11.7	0.66 ± 0.04	18.5 ± [a]
	1350	2.95 ± 0.02	355.8 ± 10.1	0.90 ± 0.10	20.5 ± 2.9
5	1200	2.01 ± 0.02	110.4 ± 3.1	1.40 ± 0.12	—[b]
	1250	2.34 ± 0.05	252.4 ± 7.5	0.94 ± 0.05	—[b]
	1300	2.72 ± 0.02	209.3 ± 4.0	0.95 ± 0.08	—[b]
	1350	2.72 ± 0.04	251.5 ± 2.8	1.50 ± 0.10	—[b]
10	1100	2.55 ± 0.02	220.5 ± 3.6	0.58 ± 0.08	31.1 ± 1.9
	1150	2.09 ± 0.02	74.4 ± 1.2	0.84 ± 0.11	27.9 ± 2.9
	1200	2.38 ± 0.02	146.2 ± 5.4	1.23 ± 0.12	30.6 ± 1.2
	1250	2.50 ± 0.04	210.0 ± 7.1	0.61 ± 0.18	11.2 ± 8.5
25	1050	2.19 ± 0.05	125.0 ± 7.9	1.76 ± 0.15	25.3 ± 3.9
	1100	2.38 ± 0.01	156.3 ± 7.6	1.39 ± 0.15	40.9 ± 10.2
	1150	2.59 ± 0.01	240.3 ± 2.9	1.47 ± 0.08	33.5 ± 5.3
	1200	2.61 ± 0.01	227.8 ± 8.3	0.87 ± 0.10	35.4 ± 3.9
50	600	1.77 ± 0.01	48.6 ± 3.2	0.83 ± 0.07	21.4 ± 2.1
	700	1.80 ± 0.01	78.1 ± 2.4	0.56 ± 0.09	31.1 ± 8.7
	800	2.17 ± 0.01	195.3 ± 8.4	1.03 ± 0.14	33.5 ± 4.8
	900	1.91 ± 0.01	67.6 ± 2.0	1.39 ± 0.07	33.0 ± 3.6

[a]Sample size too small.
[b]Measurement not possible due to radial cracking of discs on sintering.

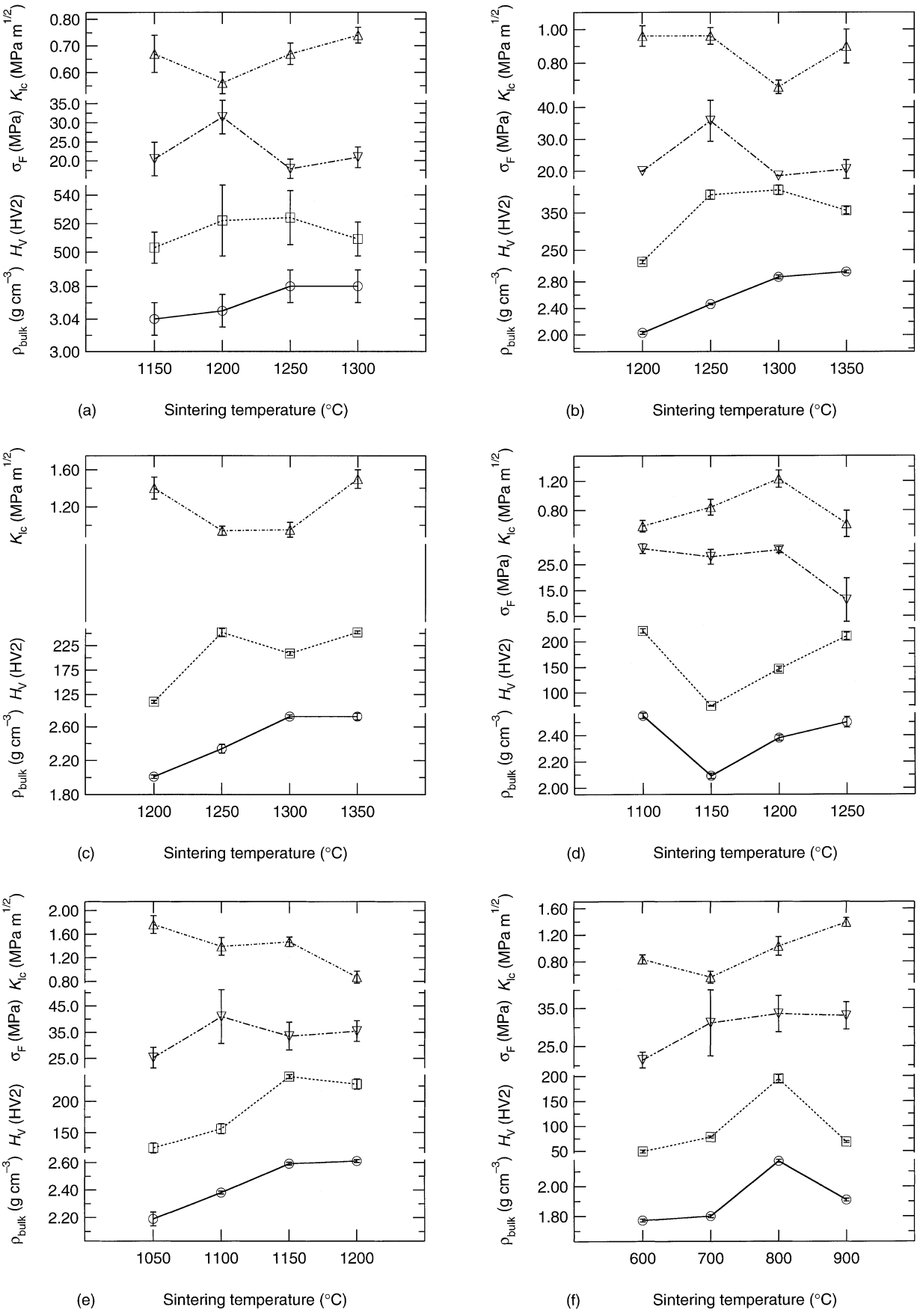

Figure 6 Variation of bulk density and mechanical properties, for both (a) pure HA, and HA/glass composites containing additions of (b) 2.5, (c) 5, (d) 10, (e) 25, and (f) 50 wt % bioglass (with 95% confidence intervals).

porosity, (ii) incorporate HA into the glass to give a constant glass composition across specimens, and (iii) have a constant mean density for all the crystalline phases, then the difference in density between the rule-of-mixtures value and the observed value, normalized for glass content,

$$\Delta\rho_{norm} = (\rho_{max} - \rho_{theor})(1 - x_{glass}) \quad (8)$$

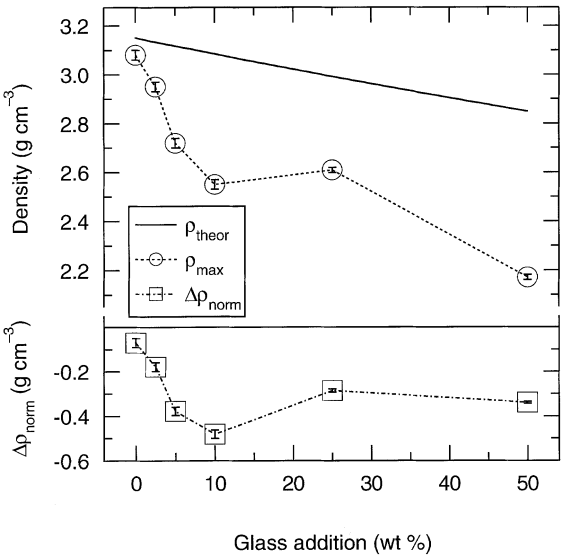

Figure 7 Variation with glass addition of maximum sintered density for each composite material (with 95% confidence intervals).

should be a constant. This value is also shown in Fig. 7, and it highlights the anomalous behavior of the 5 wt % and 10 wt % glass materials, which have densities substantially below the values expected. Note that the line is not truly horizontal, instead falling gradually with increasing glass content, and this may be accounted for by either (i) the formation of phases with lower density than HA, such as β-TCP ($\rho = 3.07\,g\,cm^{-3}$, PDF card No. 9-169), or (ii) higher porosity levels in composites containing more glass, or both.

3.3. Microstructure

Glass additions of 2.5 and 5 wt % resulted in HA matrices containing appreciable amounts of either β-TCP or α-TCP. Microstructural analysis of series containing 10 wt % glass or greater was particularly difficult due to the lack of complete X-ray phase determination and the glassy nature of the composites. Instead, for these compositions fracture surfaces were examined, to study the development of the microstructure during sintering and the nature of fracture.

3.3.1. 2.5 and 5 wt % glass additions

Figs 8 and 9 show that as the amount of glass was increased from 2.5 to 5 wt %, there was an increased amount of pore formation, which severely disrupted sintering and prevented densification. An acicular grain structure within the porous regions was observed above 1300 °C, and grew with increasing temperature.

3.3.2. 10 wt % glass addition

The fracture surfaces of samples containing 10 wt % glass, sintered at 1100 °C, showed a high degree of fine interconnecting microporosity. Higher sintering temperatures resulted in improved density but caused a gradual coarsening of the microstructure, as well as an increase in the size of the porosity. Fig. 10 shows the fracture surfaces for materials sintered at 1100 °C and 1200 °C. Sintering at 1150 °C resulted in fracture surfaces

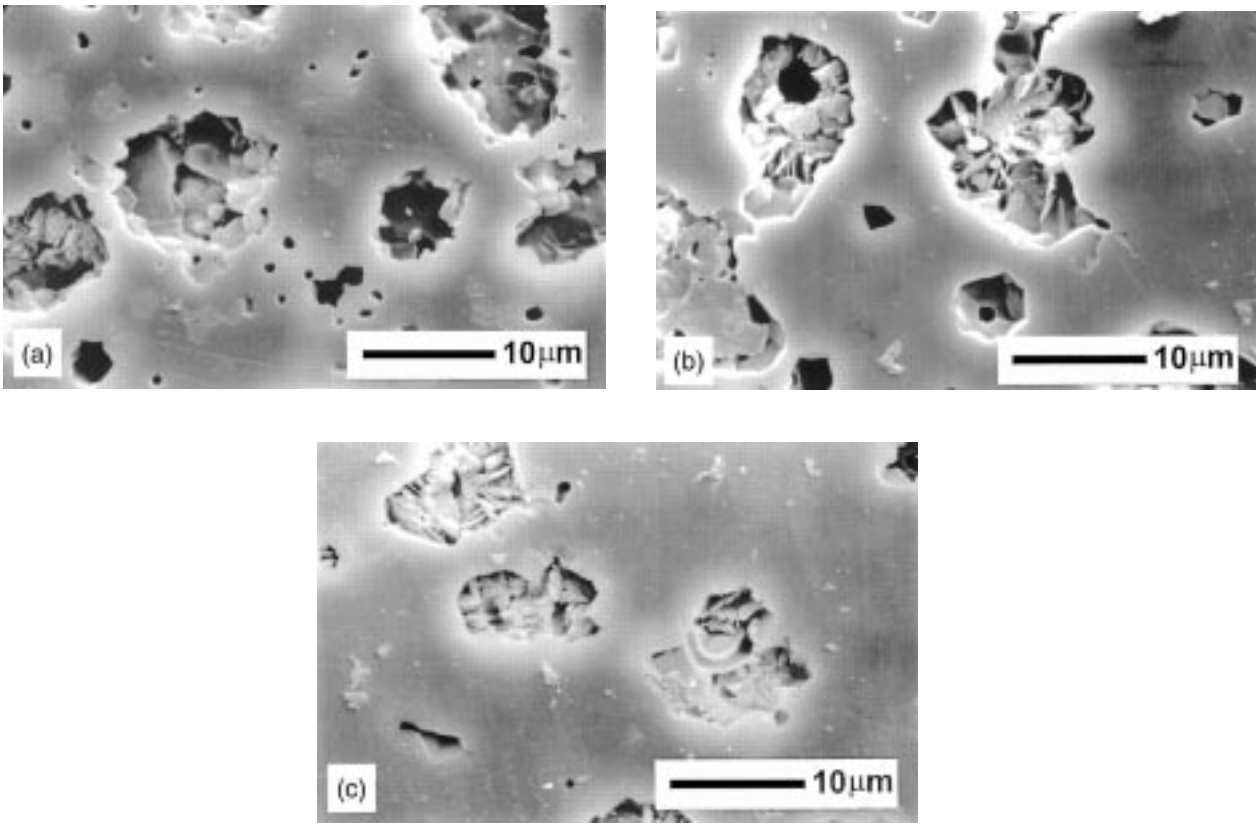

Figure 8 Development of the microstructure of 2.5 wt % bioglass composites with temperature; (a) 1250 °C, (b) 1300 °C, (c) 1350 °C.

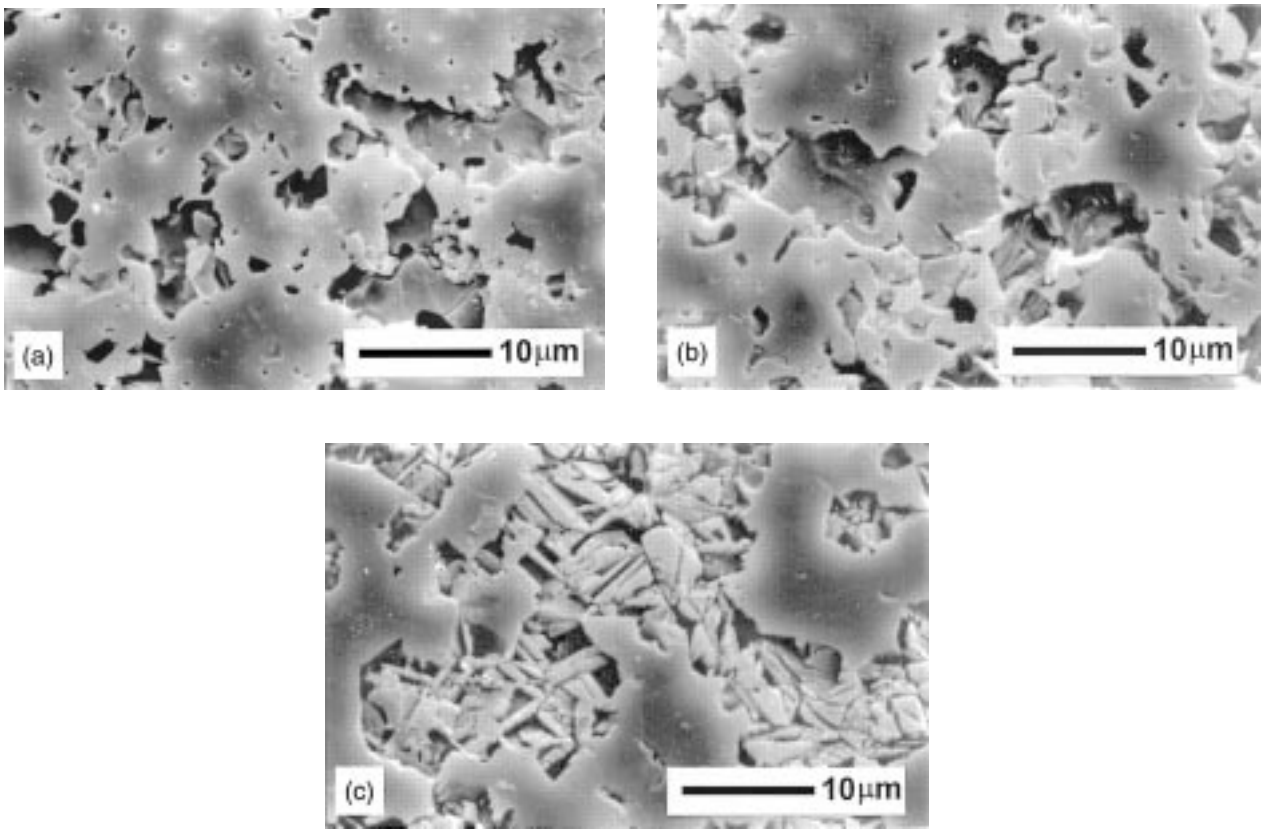

Figure 9 Development of the microstructure of 5 wt % bioglass composites with temperature; (a) 1250 °C, (b) 1300 °C, (c) 1350 °C.

intermediate between the structures shown. At the highest sintering temperature, 1250 °C, there was evidence of structural deterioration at the surface of the specimens, possibly due to localized melting of the composite. This deterioration took the form of a crazed surface and was visible to the naked eye.

3.3.3. 25 and 50 wt % glass additions

Fig. 11 shows the change in fracture surface for the 25 wt % glass series between 1050 °C and 1100 °C. Sintering at 1100 °C considerably reduced the level of fine porosity, but led to the formation of larger pores up to about 5 μm diameter. This was accompanied by the development of a locally dense glassy matrix. Fracture surfaces for higher sintering temperatures were similar, but showed a gradual increase in pore size up to about 10 μm at 1200 °C.

Although XRD did not permit identification of all phases, it was evident that large phase changes did occur for all composites based on high glass additions. Comparison of the fracture surfaces of samples sintered at 600 °C and 700 °C showed that the type of fracture changed from intergranular to transgranular. Although there was substantial microporosity present, the sintered body was locally dense with a structure similar to that for 25 wt % glass materials sintered at 1100 °C. There was little change in appearance between 700 °C and 800 °C; however, sintering at 900 °C caused a dramatic increase in the size and extent of porosity.

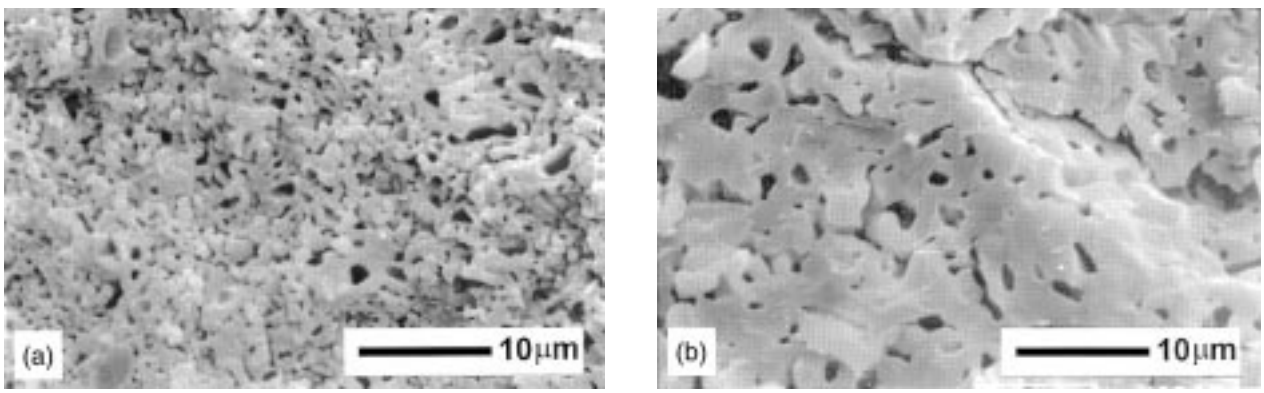

Figure 10 Fracture surfaces of HA/10 wt % bioglass composites as a function of sintering temperature: (a) 1100 °C, (b) 1200 °C.

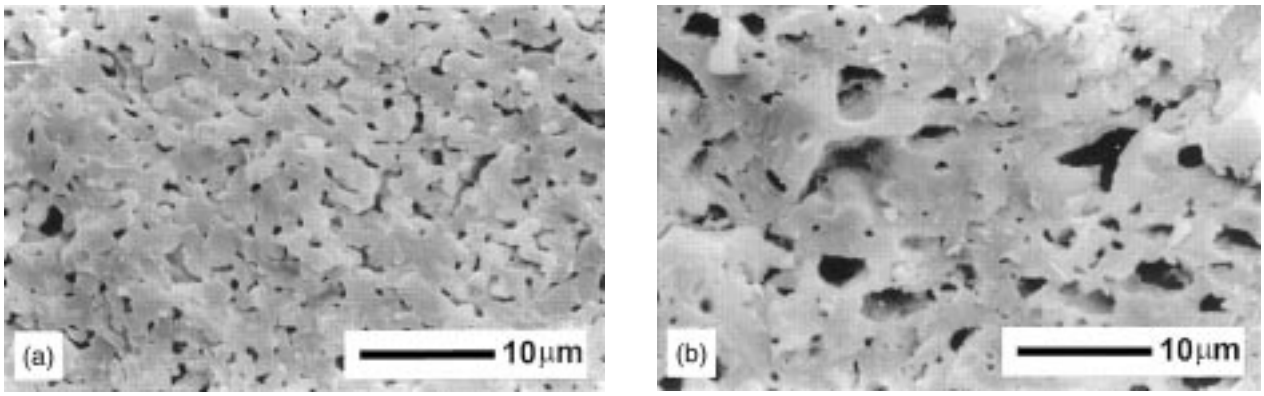

Figure 11 Fracture surfaces of HA/25 wt % bioglass composites as a function of sintering temperature: (a) 1050 °C, (b) 1100 °C.

3.4. Mechanical properties

3.4.1. 2.5 and 5 wt % glass additions

The series containing 2.5 and 5 wt % glass produced badly radially-cracked specimens upon sintering, resulting in small sample sizes for the 2.5 wt % materials, and preventing flexural testing for the 5 wt % materials; these cracks did not occur in compositions based on higher glass additions. Cracking was more severe for 5 wt % glass additions, and was also worse for samples sintered at higher temperatures. Nevertheless, the 2.5 wt % glass composites had strengths very similar to the pure HA control (Table II).

For the 2.5 wt % series, fracture toughness remained virtually constant (at just under 1 MPa $m^{1/2}$) with varying sintering temperature, the exception being the 1300 °C material, for which K_{Ic} fell significantly (Fig. 6(b)). The maximum toughness achieved (for the 1200 °C material) was almost 30% higher than for the best HA results (1300 °C), as shown in Fig. 12. The K_{Ic} of 5 wt % materials fell over the range T_{sinter} = 1250–1300 °C, but the maximum toughness (at T_{sinter} = 1350 °C) was more than twice that of the highest HA value (Fig. 12(c)).

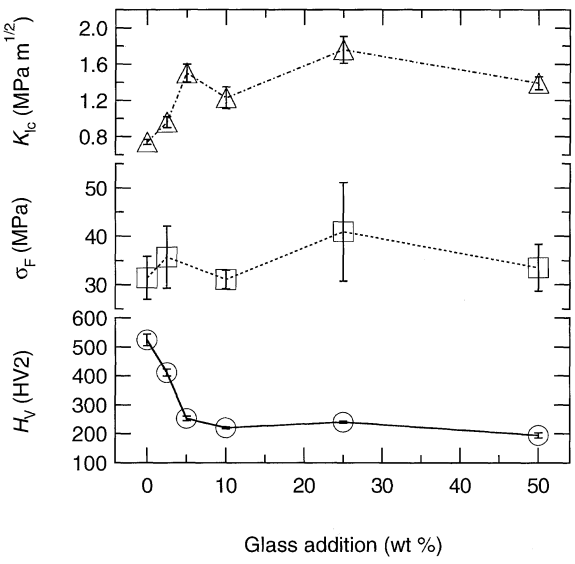

Figure 12 Variation in maximum values of mechanical properties with glass addition, over all sintering temperatures (with 95% confidence intervals).

As a general trend, hardness rose with increasing sintering temperature. The 2.5 wt %, 1350 °C, and the 5 wt %, 1300 °C materials, both had slightly low H_V values. For the most part, hardness fell with increasing glass content, the best 2.5 wt % materials being only three-quarters the hardness of the hardest HA samples, and the best 5 wt % samples reaching only half the hardness of the hardest HA (Fig. 12).

3.4.2. 10 wt % glass addition

Flexural strength was constant with T_{sinter}, except for the 1250 °C material, which may have been due to changes in the microstructure due to incipient melting. Generally, strengths were not significantly different to those of HA or the 2.5 wt % materials.

The 10 wt % materials had fracture toughnesses which were generally somewhat below those of the lower glass materials, although not as low as those of HA. The trend was for K_{Ic} to rise, and, as with σ_F, then fall at the maximum sintering temperature.

Vickers hardness varied in a somewhat unusual fashion, with an extreme fall at a sintering temperature of 1150 °C, followed by a rise with a further increase in temperature. This behavior followed the density exactly (Fig. 6(d)), and it is well-known that hardness is highly dependent upon porosity [27]. Apart from the 1150 °C material, hardness was only slightly lower than for the 5 wt % glass composites, and was substantially lower than for the HA and 2.5 wt % glass materials.

3.4.3. 25 and 50 wt % glass additions

These materials had strengths that were statistically invariant with sintering temperature, with the exception in both cases of the material sintered at the lowest temperature. Strengths of both of these series were not substantially better than HA, or any of the other composites.

For the 25 wt % series, K_{Ic} fell with increasing sintering temperature; however, the 50 wt % glass materials tended to increase in toughness as T_{sinter} rose, with a slight dip associated with the 700 °C material (associated with a change in the appearance of the fracture surface, which appeared to be more intergranular). The fracture toughnesses of the 25 wt % glass composites were generally the highest of all the

materials, even that of the worst, sintered at 1200 °C, being significantly higher than that of the best HA.

Composites containing 25 wt % glass had hardnesses that rose with sintering temperature, and were broadly similar to the 5 wt % and 10 wt % glass series. The 50 wt % composites were substantially softer than all the other materials, with an anomalously large value (although still low) for the 50 wt %, 800 °C samples; as with the 10 wt % series, the hardness trend followed the density almost perfectly.

3.5. Correlation analysis

Minitab was used to examine linear correlations between glass content, sintering temperature, bulk density, hardness, fracture toughness, flexural strength, and HA and β-TCP phase contents (both uncorrected and corrected for glass addition), using a data set composed of measurements for both pure HA and all the composites. The Pearson product moment correlation coefficients for each pairing of parameters are given in Table III.

As can be seen, there was a strong negative correlation between ρ_{bulk} and added glass content ($p < 0.0002$), but this is to be expected due to the lower density of the glass, and does not necessarily reflect on the effect of glass additions on porosity levels. Replacing ρ_{bulk} with ρ_{bulk}/ρ_{theor} (i.e., compensating for the lower density of the glass by expressing the density as fraction of the rule-of-mixtures value) gave a rather poorer correlation, although still significant ($p < 0.004$, $r = -0.57$).

There was a very strong positive correlation ($p < 0.0001$) between ρ_{bulk} and T_{sinter}, indicating that densities tended to increase as the sintering temperature rose; again, expected, except for the behavior of certain materials such as the 50 wt %, 900 °C composite, where density fell significantly.

An extremely significant ($p < 0.0001$) positive relationship was found between ρ_{bulk} and H_V, which would be normal if the lower densities were due entirely to porosity [27]; however, higher densities in these materials were also indicative of a large HA content, which may be substantially harder than the other phases present (see below). An additional correlation test between ρ_{bulk}/ρ_{theor} and H_V was still highly significant ($p < 0.0001$, $r = 0.86$), confirming that high porosity, and the formation of lower-density phases other than glass, were responsible for reducing the hardness.

There was a large, positive correlation between ρ_{bulk} and the mass fraction of HA present after sintering, probably due to the high density of HA compared to all the other phases in the system. This relationship became weaker (although still significant at $p < 0.005$) when the glass content was compensated for (HA corr.).

Hardness strongly negatively correlates with added glass content, as would be expected due to the replacement of the harder, crystalline HA, with the softer bioglass. There was a weaker relationship between H_V and T_{sinter}, but this was due to the increase in ρ_{bulk} with T_{sinter}. Interestingly, there was an extremely strong positive correlation ($p < 0.0001$) between H_V and HA content, but no such relationship existed with β-TCP, indicating that HA was overwhelmingly the principal contributor to the hardness, in polyphase mixtures.

Neither fracture toughness nor flexural strength correlate strongly with any other parameter, the strongest relationship for K_{Ic} being a weak negative correlation ($p = 0.03$) with H_V, which was not abnormal, harder materials tending to be more brittle. The strongest link between flexural strength and any other variable was a weak negative correlation with HA content (even less so with the corrected HA content), at $p = 0.03$.

4. Discussion

Composites containing additions of up to 5 wt % bioglass consisted of HA, with β-TCP as the secondary phase up to 1250 °C, and with α-TCP at higher sintering temperatures. There was no evidence in XRD of any crystalline phase directly related to the added bioglass, for example calcium phosphate silicate [11], rhenanite, or wollastonite [10]. However, the lattice parameters of both HA and β-TCP showed that significant deviations from stoichiometry did occur, indicating possible dehydroxylation of HA or substitution of ions from the glass. Comparison with an earlier study of composites based on similar additions of a phosphate glass [3] shows that, in general, changes in lattice parameters resulting from bioglass additions were larger, indicating a greater deviation from stoichiometry or higher levels of substitution. Although the HA/TCP ratio was similar between the phosphate glass and

TABLE III Pearson product moment correlation coefficients (r) for composition, processing, and property variables, for all HA and HA/ bioglass materials. Coefficients for variables known to be strongly dependent have been removed

	Glass	T_{sinter}	ρ_{bulk}	H_V	K_{Ic}	σ_F	HA	β-TCP	HA corr.	β-TCP corr.
ρ_{bulk}	−0.69**	0.70**								
H_V	−0.66**	0.56*	0.89**							
K_{Ic}	0.22	0.00	−0.32	−0.45						
σ_F	0.40	−0.26	−0.28	−0.31	0.42					
HA	−0.71**	0.52*	0.66**	0.83**	−0.40	−0.45				
β-TCP	−0.07	0.01	−0.22	−0.31	−0.12	0.20	−0.34			
HA corr.	−0.53*	0.33	0.55*	0.77**	−0.43	−0.42	—	−0.38		
β-TCP corr.	−0.07	0.01	−0.22	−0.31	−0.12	0.20	−0.34	—	−0.38	
HA/β-TCP	0.18	−0.32	−0.29	0.02	−0.15	0.22	—	—	—	—

* Denotes $p < 0.01$, ** $p < 0.001$.

bioglass composites, α-TCP formed at about 50 °C lower, and in greater quantities, for bioglass-containing composites.

Glass additions of up to 5 wt % led to considerable disruption of sintering, delaying densification to higher temperatures. Sample densities were considerably below values for HA sintered at the same temperature and well below corresponding values for composites of HA/phosphate glass [3, 11]. It is likely that the high porosity resulted from reaction between the bioglass and HA. The emergence and growth of an acicular grain structure above 1300 °C may correspond to the observed formation and growth of α-TCP over the same temperature range.

Flexural strength data was restricted for the 2.5 wt % glass, and not available at all for the 5 wt % glass materials, due to cracking of samples during sintering. The available data indicate that no significant improvement in strength over HA was obtained. The reasons for sample cracking are uncertain, and variation of pressing pressure, binder/lubricant content, and heating rate, did not eliminate it. Volumetric change associated with the formation of β-TCP and α-TCP did not appear to be solely responsible – equally large phase changes for composites based on phosphate glass samples did not result in cracking [3, 11]. Figs 8 and 9 show the formation of large porous regions about 10 μm in diameter. Due to the approximately spherical nature of the pores, they may have resulted due to gas entrapment, possibly arising due to OH^- release on decomposition of HA [18, 28, 29]. Cracking may have resulted from the stresses caused by expansion due to the formation of lower-density phases, and local stresses due to gas evolution following densification. A previous study by Santos *et al.* [11] in which HA was sintered with a Hench-type bioglass (of slightly different composition to that used in the present work) found similar poor densification of composites. Cracking of specimens at 1350 °C was also observed. Mechanical testing in the same study showed that although strengths were comparable to, or showed a small improvement over, HA, the extent of improvement was significantly below that obtained for other types of glass addition.

Hardness of the composites declined rapidly with increasing glass additions, from 0 → 2.5 → 5 wt %, tending to follow the reduced density of the materials. Fracture toughness, however, was found to increase substantially, which may have useful implications for load-bearing parts to be used in the body. Whether the improved K_{Ic} is due to the presence of either α- or β-TCP, or due to crack-blunting by the pores, or through some limited plasticity or crack-deflection associated with the glass, is unclear.

Due to poor densification, as well as the formation of the more rapidly resorbable α-, rather than β-TCP, at higher temperatures, it seems unlikely that composites based on low bioglass additions offer a mechanical advantage as a biomaterial over either traditional biphasic HA/TCP composites [29] or HA/phosphate glass composites [1, 3]. However, despite this, small bioglass additions to hydroxyapatite may allow preparation of composites with useful bioactive properties. Similar composites have previously been shown to be capable of more rapid formation of a calcium phosphate surface layer than HA, *in vitro* [12]. Knowledge of the phase composition, stoichiometry, and sintering characteristics of these composites, will aid understanding of their resorption characteristics and prediction of the likely biological response.

Higher glass additions disrupted sintering, compared to pure HA, resulting in poor densification; however, no cracking of specimens occurred. Despite very high porosity, flexural strengths for each series did not differ significantly from the maximum strength measured for HA. Complete phase analysis by XRD for high bioglass-containing composites was made impossible due to peak broadening and overlap, coupled with the formation of a number of additional, apparently low-symmetry, phases. Despite the problems with phase identification, sufficient analysis was possible to show that substantial degradation of the HA occurred at all temperatures, especially for the 50 wt % glass materials at sintering temperatures as low as 600 °C. For the 50 wt % materials at the two highest sintering temperatures, β-$Na_2Ca_4(PO_4)_2SiO_4$ was tentatively identified as being present, and wollastonite-2M was another possible phase identified in the material with the highest T_{sinter}, 900 °C: no HA was present at all in that material, indicating complete reaction. Kangasniemi *et al.* [10, 14, 18, 30] observed no reaction between HA and bioglass in their materials sintered at 600 °C; however, the HA particles were considerably coarser than those used in the present study, reducing the interfacial area over which reaction could occur. Lower densification in this work may be attributed to reaction between bioglass and HA, resulting in the formation of pores and lower-density phases, and to use of much lower glass additions.

Despite the poor densification, and high level of reaction between HA and glass, flexural strengths of these materials were not very different to those for pure HA. Fracture toughness fell markedly for the 10 wt % glass materials as a whole, recovered to exceptionally high levels at 25 wt % glass (about twice the values for pure HA), and then declined again with the 50 wt % specimens. Hardnesses tended to be stable for the 10 and 25 wt % bioglass composites, after the rapid fall over the range 2.5 to 5 wt % glass. The hardness then tended to reduce for the 50 wt % glass series.

Linear correlations observed over the whole range of materials, from pure HA to 50 wt % bioglass composites, were:

1. Bulk density and fraction of maximum theoretical density decreased with increasing glass content.
2. Specimens with high bulk densities tended to have high HA contents after sintering.
3. Hardness decreased with increasing glass additions and decreasing bulk density.
4. Hardness increased with the amount of HA in the sintered product, but was independent of β-TCP content.
5. Fracture toughness did not correlate well with any other variable, nor did flexural strength. There does, however, appear to be a non-linear correlation between K_{Ic} and glass content, with a maximum K_{Ic} being obtained at 25 wt % glass.

The likely biological behavior of the high bioglass-containing composites has not yet been clearly established. The bioactivity of some similar composites has previously been investigated, both as plasma sprayed coatings [6, 7] on titanium implants, and as dense implants [14, 30]. *In vitro* [7, 14, 30] and *in vivo* [15, 16] testing has indicated that HA-composite materials based on high bioglass additions are bioactive, developing a calcium phosphate surface layer, and could bond directly to bone. However, due to differences in material preparation, composition, and form of implant between these studies, it is not possible to comment on the likely biological behavior of composites based on high bioglass additions prepared in the present work, without suitable testing.

5. Conclusions

The sintering, compositional, and mechanical properties of HA/bioglass composites containing 0–50 wt % glass additions were established. Low glass additions resulted in the formation of either HA/β-TCP or HA/α-TCP, depending on sintering temperature. In general, sintering was disrupted by the presence of bioglass, limiting densification, or delaying it to higher temperatures. Although flexural strengths showed no improvement over HA, and hardness declined with increasing glass content, significant gains in fracture toughness were observed, particularly for the materials with 25 wt % bioglass, which were more than twice as tough as HA. However, no significant mechanical advantage was identified over traditional biphasic calcium phosphates and mechanical properties were significantly poorer than those of composites based on similar additions of phosphate glasses.

Dedication

To the memory of Caroline Healy. An undergraduate student of mechanical engineering at UCD, she expressed an enthusiastic interest in materials. Her life was tragically cut short, aged 21, at the time that the authors were preparing the final draft of this paper.

Acknowledgments

This research was partially funded by Forbairt (the Government Agency for Enterprise, Innovation, Investment, and Development) through the Applied Research Grant program.

Additional support for DCT was provided by IDA Ireland, under the Newman Scholarship scheme.

References

1. J. C. KNOWLES and W. BONFIELD, *J. Biomed. Mater. Res.* **27** (1993) 1591.
2. J. C. KNOWLES, *Br. Ceram. Trans.* **93** (1994) 100.
3. D. C. TANCRED, B. A. O. MCCORMACK and A. J. CARR, *Biomaterials* **19** (1998) 1735.
4. J. D. SANTOS, P. L. SILVA, J. C. KNOWLES, S. TALAL and F. J. MONTEIRO, *J. Mater. Sci. Mater. Med.* **7** (1996) 187.
5. A. AFONSO, J. D. SANTOS, M. VASCONCELOS, R. BRANCO and J. CAVALHEIRO, *ibid.* **7** (1996) 507.
6. J. H. CHERN LIN, M. L. LIU, K. S. CHEN and C. P. JU, in ''Ceramic Engineering and Science Proceedings'', vol. 14 (1993).
7. J. H. CHERN LIN, M. L. LIU and C. P. JU, *J. Biomed. Mater. Res.* **28** (1994) 723.
8. S. BAN, S. MARUNO, H. IWATA and H. ITOH, *ibid.* **28** (1994) 65.
9. N. YAMASAKI, K. YANAGISAWA and N. KAKIUCHI, *J. Mater. Res.* **5** (1990) 647.
10. I. KANGASNIEMI, K. DE GROOT, J. WOLKE, Ö. ANDERSSON, Z. LUKLINSKA, J. G. M. BECHT, M. LAKKISTO and A. YLI-URPO, *J. Mater. Sci. Mater. Med.* **2** (1991) 133.
11. J. D. SANTOS, J. C. KNOWLES, R. L. REIS, F. J. REIS, F. J. MONTEIRO and G. W. HASTINGS, *Biomaterials* **15** (1994) 5.
12. J. D. SANTOS, L. J. JHA and F. J. MONTEIRO, *J. Mater. Sci. Mater. Med.* **7** (1996) 181.
13. J. D. SANTOS, L. J. JHA and F. J. MONTEIRO, *Biomaterials* **16** (1995) 521.
14. I. M. O. KANGASNIEMI, ''Development of Ca,P-Ceramic Containing Bioactive Glass Composites'', Master's thesis, University of Leiden, The Netherlands (1993).
15. E. SUOMINEN, A. J. AHO, E. VEDEL, I. KANGASNIEMI, E. UUSIPAIKKA and A. YLI-URPO, *J. Biomed. Mater. Res.* **32** (1996) 543.
16. E. A. SUOMINEN, A. J. AHO, J. JUHANOJA and A. YLI-UPRO, *Int. Orthop.* **19** (1995) 167.
17. H. TAGAI and H. AOKI, in ''Mechanical Properties of Biomaterials'', edited by G. W. Hastings and D. F. Williams (Wiley, New York, 1980), pp. 447–488.
18. I. M. O. KANGASNIEMI, K. DE GROOT, J. G. M. BECHT and A. YLI-URPO, *J. Biomed. Mater. Res.* **26** (1992) 663.
19. C. CHATFIELD, ''Statistics for Technology'', revised 3rd edn. (Chapman & Hall, London, 1996).
20. S. WESTMAN and A. MAGNÉLI, *Acta Chem. Scand.* **11** (1957) 1587.
21. H. P. KLUG and L. E. ALEXANDER, ''X-ray Diffraction Procedures for Polycrystalline and Amorphous Materials'', 2nd edn. (Wiley-Interscience, New York, 1974).
22. H. L. MONACO, in ''Fundamentals of Crystallography'', edited by C. Giacovazzo (International Union of Crystallography and Oxford University Press, Oxford, 1992), pp. 297–301.
23. R. L. SNYDER, in ''X-ray Characterization of Materials'', edited by E. Lifshin (Wiley-VCH, Weinheim, Germany, 1999) pp. 73–83.
24. M. U. COHEN, *Rev. Sci. Instrum.* **6** (1935) 68.
25. D. J. GODFREY and S. JOHN, in ''Ceramic Materials and Components for Engines'', edited by W. Bunk and H. Hausner (Deutsche Keramische Geselleschaft, Bad Honnef, 1986), pp. 657–665.
26. B. R. LAWN and E. R. FULLER, *J. Mater. Sci.* **10** (1975) 2016.
27. R. W. RICE, in ''Treatise on Materials Science and Technology: Properties and Microstructure'', edited by R. K. MacCrone, vol. 11 (Academic Press, New York, 1977), pp. 328–329.
28. A. J. RUYS, M. WEI, C. C. SORRELL, M. R. DICKSON, A. BRANDWOOD and B. K. MILTHORP, *Biomaterials* **16** (1995) 409.
29. A. ROYER, J. C. VIGUIE, M. HEUGHEBAERT and J. C. HEUGHEBAERT, *J. Mater. Sci. Mater. Med.* **4** (1993) 76.
30. I. M. O. KANGASNIEMI, E. VEDAL, J. DEBLICK-HOGERWORST, A. U. YLI-URPO and K. DE GROOT, *J. Biomed. Mater. Res.* **27** (1993) 1225.

Received 9 September 1998
and accepted 2 December 1999